

## Comparison of unitary and hybrid cement systems activated with acid and alkaline solutions

*Comparação de sistemas cimentícios unitários e híbridos ativados com solução ácida e solução alcalina*

Madeleing Taborda-Barraza 

Vanessa de Amorim Amorim 

Thais Marques da Silva 

Philippe Jean Paul Gleize 

### Abstract

In parallel with the alkaline activation of aluminosilicates, acid activation takes place. Often less studied, the so-called phosphate-based geopolymers are little publicized due to the concerns that arise during their manufacture. However, they are presented as materials with greater mechanical strength and greater chemical stability than alkaline activations. Thus, their applications are not as simple as forming structural parts, but in specific applications that do not require an integral core. The acidic and alkaline activation of metakaolin and fly ash was evaluated in the fresh and hardened state using calorimetry, mini-slump, rotational rheology and compressive strength. For unitary systems, acid activation presented greater compressive strength than alkaline activation. However, for hybrid systems there was a limitation in the incorporation of fly ash, which, over time, favored the mechanical behavior of alkaline systems over acids systems.

**Keywords:** Activation. Acid. Alkaline. Strength. Metakaolin. Fly-ash.

### Resumo

Paralelamente à ativação alcalina dos aluminossilicatos ocorre a ativação ácida. Frequentemente menos estudada, os chamados geopolímeros à base de fosfato são pouco divulgados devido às considerações em relação a sua fabricação. Entretanto, apresentam-se como materiais com maior resistência mecânica e maior estabilidade química que os resultantes de ativações alcalinas. Assim, suas aplicações não são tão simples como a conformação de peças estruturais, mas sim em aplicações específicas que não necessitam de núcleo integral. A ativação ácida e alcalina do metacaulim e da cinza volante foi avaliada no estado fresco e endurecido por meio de mini-slump, reologia rotacional e resistência à compressão. Para sistemas unitários, a ativação ácida conferiu maior resistência à compressão que a ativação alcalina em geopolímeros. Porém, para sistemas híbridos houve limitação na incorporação da cinza volante, que com o tempo favoreceu o desempenho mecânico dos sistemas alcalinos e não aos sistemas ácidos.

**Palavras-chave:** Ativação. Ácida. Alcalina. Resistência. Metacaulim. Cinza volante.

<sup>1</sup>Madeleing Taborda-Barraza  
<sup>1</sup>Universidade Federal de Santa Catarina  
Florianópolis - SC - Brasil

<sup>2</sup>Vanessa de Amorim Amorim  
<sup>2</sup>Universidade Federal de Santa Catarina  
Florianópolis - SC - Brasil

<sup>3</sup>Thais Marques da Silva  
<sup>3</sup>Universidade Federal de Santa Catarina  
Florianópolis - SC - Brasil

<sup>4</sup>Philippe Jean Paul Gleize  
<sup>4</sup>Universidade Federal de Santa Catarina  
Florianópolis - SC - Brasil

Recebido em 03/05/24  
Aceito em 19/08/24

## Introduction

Acid activation of calcined clays for cementitious purposes is a relatively recent approach compared to traditional alkaline activation (Gao *et al.*, 2020; Tchakouté; Rüschler, 2017). However, it's noteworthy that the insolubility of the products formed by this technique was already recognized in agronomy. Agricultural studies revealed that mixing phosphate fertilizers with acidic soils, especially clayey ones, led to the formation of hardened and insoluble soil, which were unsuitable for agriculture (Medina; Guida, 1995). Moreover, laterite soils, prevalent in tropical regions and rich in iron and aluminum oxides, have found application in civil engineering. These soils can be stabilized with phosphoric acid, making them suitable for various purposes, like soil stabilization for roads and paving (Eisazadeh; Kassim; Nur, 2012; Michaels; Tausch, 1961). For application purposes in civil engineering, the activation of metakaolin (MK) using  $H_3PO_4$  still registered at limited literature (Alvi *et al.*, 2024; Derouiche; Baklouti, 2021)

According to Pereira (2003), the ionic exchange between the structural interlayer cations of clays and the acid's anions during acid activation results in significant changes in the crystalline structure and original properties of clays. These structural and property changes can lead to different characteristics of the final products, depending on the specific chemical composition of the clay and the type of acid used. For instance, products may exhibit properties like adsorption or filtration capacity (Le-Ping *et al.*, 2010). The ability to adjust the characteristics of final products by varying the chemical composition of clay and acid opens up possibilities for applications in different fields, such as the development water purification adsorbents or industrial effluent treatment filters.

Geopolymerization produces an inorganic polymer developed by similar reaction kinetics in acid or basic environment. The acid-based polymerization reaction involves the bonding of Al–O (from metakaolin) and P–O tetrahedral units (from  $H_3PO_4$  solution) (Alvi *et al.*, 2024).  $[AlO_4]^{5-}$ ,  $[SiO_4]^{4-}$ , and  $[PO_4]^{3-}$  are the fundamental groups evolving into acid activation by phosphoric acid, where  $[PO_4]^{3-}$  ions replace alkali metal ions in alkaline systems (Li *et al.*, 2022). Louati, Baklouti and Samet (2016) indicate that the positive charges of ionized  $H_3PO_4$  are balanced with  $[AlO_4]^{5-}$ , as the positive charges of dissociated NaOH are balanced by  $[AlO_4]^{5-}$  (Pacheco-Torgal *et al.*, 2015). Thus, the bonds formed are of the Si type /Al - O - P. Furthermore, the degree of polymerization is influenced by factors like the Si/P molar ratio and curing temperature, similar to alkaline systems (Zribi; Samet; Baklouti, 2020).

The acid activation products of aluminosilicates are also termed phosphate-based geopolymers. These composites, with high phosphate content, can be incorporated into traditional aluminosilicates with low acid concentrations to enhance reactivity. They exhibit characteristics like low efflorescence/carbonation, dimensional stability against acid attack, and proportional dielectric properties to mechanical performance (Derouiche; Baklouti, 2021). Ongoing research on these composites enables the utilization of other by-products, more specific applications, and the development of micro-nanoparticles with higher affinity in acidic environments.

## Materials and methods

Metakaolin (MK) and Fly Ash (FA) were obtained from a national industry and a thermoelectric plant, respectively. X-ray fluorescence (EDX7000, Shimadzu) was performed to determine chemical compositions and the results are shown in Table 1.

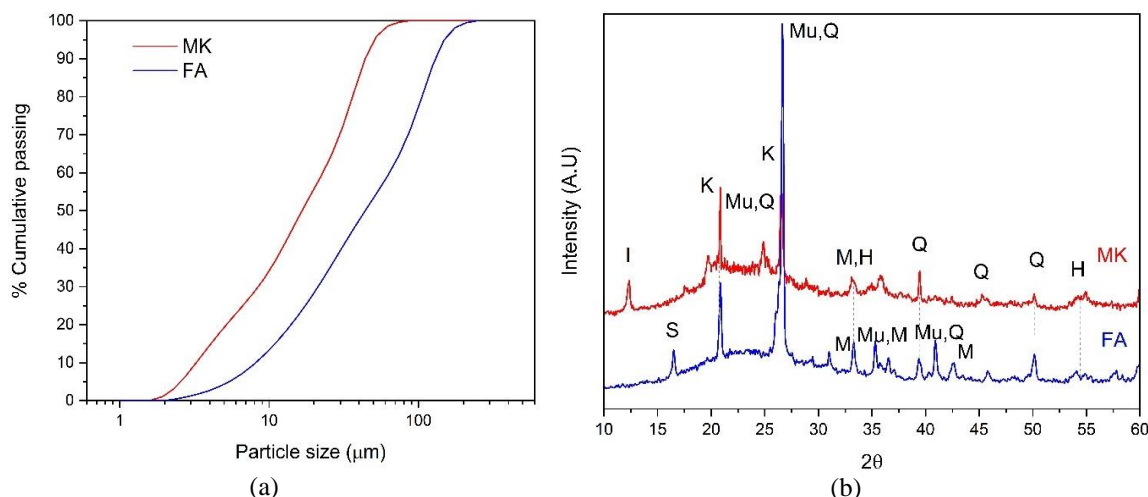
Laser diffraction (Microtrac S3500) was used to determine the particle distribution, as shown in Figure 1a. The mean diameters ( $\mu m$ ) of MK and FA were 16.26 and 51.06, respectively. The mineral phases were identified, see Figure 1b, using XRD measurement (Miniflex, Rigaku).

Table 1 - Chemical composition of precursors

-	SiO <sub>2</sub>	Al <sub>2</sub> O <sub>3</sub>	Fe <sub>2</sub> O <sub>3</sub>	CaO	MgO	K <sub>2</sub> O	Others	L.I*(%)
<b>MK (%)</b>	49.06	37.96	5.93	0.54	2.10	0.10	1.03	3.30
<b>FA (%)</b>	57.43	27.43	5.08	1.96	0.32	3.50	2.31	1.97

Legend: L.I\*= Lost ignition

Figure 1 - (a) Distribution particle size of MK and FA; and (b) XRD patterns of MK and FA



**Legend:** I: ilite; K: kaolinite; Q: quartz; Mu: Mullite; and H: Hematite.

For acid activation, phosphoric acid at a concentration of 85%, diluted into deionized water, resulting in a molar concentration of 6.12 mol/L of  $\text{H}_3\text{PO}_4$  was used. This concentration was chosen considering the highest value from He *et al.* (2023) and Tchakouté and Rüschler (2017). For alkaline activation, the solution employed was composed by sodium silicate and sodium hydroxide, getting a concentration of 6.26 mol/L of NaOH, this concentration was used by the research group (Luz *et al.*, 2019). Both solutions were prepared on a magnetic stirrer and allowed to stand for 24 hours before use. The solution was added to the power material during the mixing process according to the mass proportions specified in Table 2. The mixture was prepared using a mechanical mixer at 600 rpm for 4 minutes, tested for mini-slump test, isothermal calorimeter at 65 °C (I-Cal 2000HPC, Calmetrix), and then molded into cylinders with a diameter of 19 mm and a height of 24 mm. These molds were subsequently placed into an oven for curing at 65 °C for three days.

The rheologic measures were obtained from Haake Mars rheometer (Vane geometry – pre-shear at 50  $\text{s}^{-1}$ , rise ramp from 0.1 to 100  $\text{s}^{-1}$  and from 90 to 0.1  $\text{s}^{-1}$  for four minutes), using a similar routine used by Taborda-Barraza *et al.* (2022) and in its hardened state by the compressive strength test (Instron model 5569) press and a load rate of 4000 N/min. Furthermore, a microstructural analysis was carried out using X-ray diffraction (XRD) (Miniflex, Rigaku) and Fourier Transform Infrared Spectroscopy (FTIR) after 28 days of reaction. KBr pellets were used to prepare the samples (1 mg of sample/ 300 mg of KBr) (4200 FTIR, Jasco) based on the following parameters: analysis range of 400-4000  $\text{cm}^{-1}$ ; resolution of 160  $\text{cm}^{-1}$ ; and 52 accumulations. X-ray diffraction analysis was also applied for the samples. The precursors also were analyzing through zeta potential (Zetasizer NanoZS, Malvern).

## Results and discussion

Figure 2 shows the zeta potential at different pH for both precursors. The results indicate that raw material samples exhibited greater stability at alkaline pH levels (>7) while instability was observed at more acid pH levels.  $\pm 30\text{mV}$  indicates the most unstable zone for the particles, a state with tendency to aggregation or agglomeration (Kriegseis *et al.*, 2020). Specifically, FA samples showed less stability than MK due to their lower value of PZ modulus, i.e., a system predominantly negative charge (Gunasekara; Setunge; Sanjayan, 2015). However, their stability starts to be manifested even at lower pH (>4), and pH alkaline arrived better stabilization. Conversely, MK sample demonstrated few stabilities for acid pH values. This means that both precursors probably register precipitation and few dissolutions in acid conditions but great behavior on alkaline conditions.

## Evaluation on fresh state

The appearance of the fresh state of various samples, via mini-slump, has been documented in Figure 3. Specifically, the acid activation system was found to be easy to mix, but the consistency of the resulting mixture was firm, showing minimal spreading compared to alkaline activation. Additionally, it was observed that, as the fly ash content increased in the samples, the scattering increased in both systems. This was

attributed to spherical shape of ash particles that favor flow. Both systems shared a common trait: their final setting time tended to be longer, typically exceeding 3 days, when compared to cement systems based on Portland cement (Xie *et al.*, 2023). Consequently, thermal curing is often applied (Kaze *et al.*, 2021). This delayed setting time is a consequence of the slow dealumination of particles in acidic environments at room temperature. Similarly, in alkaline environments, a low rate of particle dissolution is observed at room temperature, particularly in mixtures with low calcium and sodium hydroxide contents.

In addition, the rheology of the pastes was evaluated, and the results were summarized in Figure 4. Both systems exhibited a reduction in viscosity as the shear rate increased, indicating pseudoplastic behavior. The representative equations for the rheological models are summarized in Table 3. Calculating the yield stress of the systems, it was noted that not all samples could be fitted into the same model. This was because the yield stress value appeared to be negative in some cases, indicating a fluid that was sufficiently easy to spread. This behavior was observed particularly when fly ash was incorporated into a hybrid system, a phenomenon also documented by (Aboulayt *et al.*, 2018).

Table 2 - Mass composition of the samples

Name (Mix)	MK (g)	FA (g)	Acid solution (g) ( $\text{H}_3\text{PO}_4\text{:H}_2\text{O}$ ) (1:0,82)
			or Alkaline solution (g) ( $\text{Na}_2\text{SiO}_3\text{: NaOH}$ ) (1:0,066)
100MK	80	-	96
80MK-20FA	64	16	96
60MK-40FA	48	32	96
40MK-60FA	32	48	96

Figure 2 - Zeta potential of MK and FA at different pH

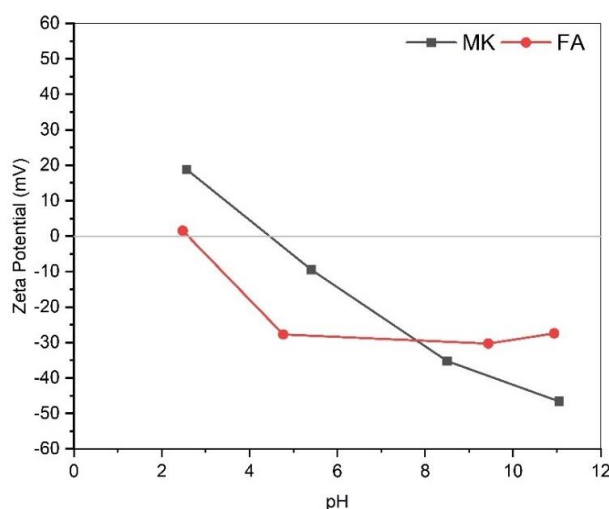






Figure 3 - Mini-slump values and appearance of some activated mixtures

Acid activation	Acid activation	Acid activation	Acid activation
100MK -slump: 64.55 mm	40MK-60FA -slump: 117.7 mm	100MK -slump: 86.50 mm	40MK-60FA -slump: 122.10 mm
			

In the analysis, representative models for each system were highlighted in yellow. Consistent with the mini-slump test, the incorporation of ash resulted in a reduction in yield stress. Both individual systems required energy with values close to each other to initiate flow within the system. When evaluating the systems using the Herschel-Bulkley model, it was found that acid activation exhibited greater consistency, indicating visual firmness. On the other hand, when assessing viscosity using the Bingham model, it was observed that alkaline activations were more viscous compared to acidic ones.

The same groups were also defined using a calorimetric test, i.e., 100MK and 40MK-60FA. The results are summarized in Figure 5. Figure 5 shows the heat flow at 65 °C (Figure 5a) and the total heat accumulated (Figure 5b). The first observation is related to the higher intensity of dissolution (Peak I) in acid systems compared with alkaline systems. This behavior was discussed by Bu *et al.* (2024), who explains that in acid environments the solubility on MK surfaces is higher compared to alkaline environments, due to Al-O bonds being weaker in this condition. Even when the presence of FA led to a reduction in this intensity for 100MK group, the dissolution value was higher than in alkaline activations. Consequently, the total heat accumulated for 40MK-60FA was reduced in 78,68% at 48 hours, compared with 100MK, after contact between precursor and activator. This phenomenon also indicated that FA did not contribute significantly to the kinetic reaction under these conditions.

The second observation is related to peak II, that appears to alkaline activated systems, nevertheless for acid systems, based on a tendency of transformation of a concave curve to a convex curve between 1-2 hours. Xie *et al.* (2023) registered a decrease in the intensity of dissolution peak when the concentration  $H_3PO_4/H_2O$  was reduced, after eight hours no peak was registered. Few studies discuss the calorimetry in acid systems. Finally, alkaline systems were negatively affected by the presence of fly ash, reducing the intensity of the dissolution peak and the final energy of the system, .

## Evaluation on hardening state

In Figure 6 the results of compressive strength are presented. It was observed that acid activations performed better in systems based on 100MK and 80MK, showing an increase of 45% and approximately 90%, respectively, compared to the same systems in alkaline activation. However, for combinations with a lower proportion of MK, such as 40FA and 60FA, alkaline activations exhibited superior performance over acid activations. The 60FA system showed zero strength, as consequence of demold failure due to soft consistency. These findings align with similar results obtained by Louati, Baklouti and Samet (2016), and Xie *et al.* (2023) for acid activation of MK. The data represented in Table 2 highlights the influence of material composition on compressive strength, with acid and alkaline activations demonstrating variable performance depending on the specific proportions of materials used.

Figure 4 - Shear stress and apparent viscosity from extreme groups

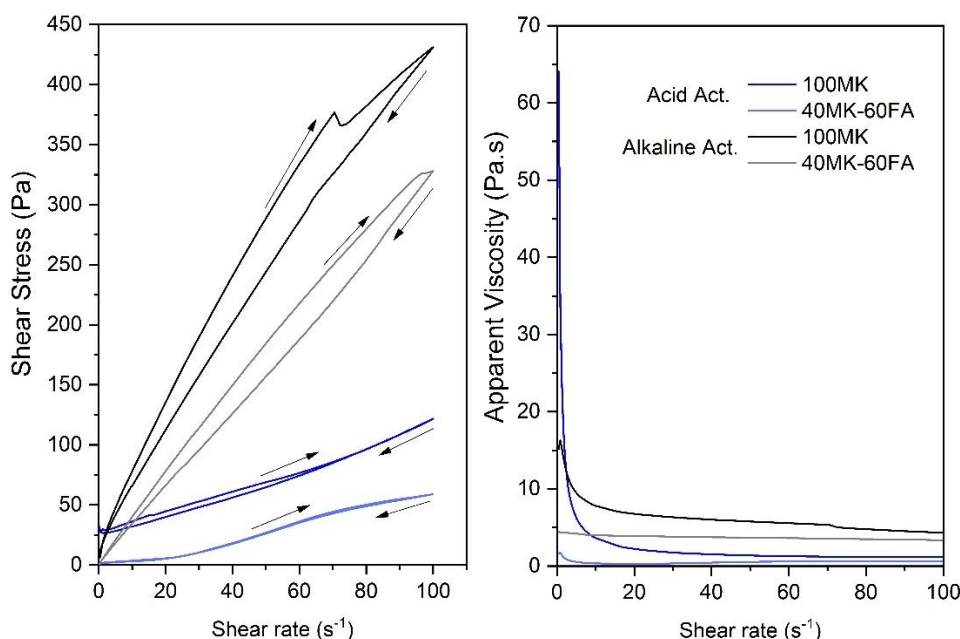


Table 3 - Rheological parameters defined

Activation type	Group	Herschel-Bulkley Model $\tau = \tau_0 + K\dot{\gamma}^n$	Bingham Model $\tau = \tau_0 + \eta_p\dot{\gamma}$
Acid	100MK	$\tau_0 = 29.22$ $K = 0.432$ $\eta = 1.16$	$\tau_0 = 26.51$ $\eta_p = 0.88$
Acid	40MK-60FA	$\tau_0 = 0.295$ $K = 0.174$ $\eta = 1.28$	$\tau_0 = -2.820$ $\eta_p = 0.63$
Alkaline	100MK	$\tau_0 = -18.93$ $K = 23.90$ $\eta = 0.65$	$\tau_0 = 38.94$ $\eta_p = 4.42$
Alkaline	40MK-60FA	$\tau_0 = -4.235$ $K = 6.16$ $\eta = 0.87$	$\tau_0 = 7.27$ $\eta_p = 3.41$

**Legend:**  $\tau_0$ : yield stress in Pa;  $\eta_p$ : plastic viscosity in Pa.s;  $\eta$ : flow index; K: consistency index in Pa.s; and  $\dot{\gamma}$ : shear rate in s<sup>-1</sup>.

Figure 5 - Reaction kinect for 100MK and 40MK-60FA groups in the first 48 hours - (a) Heat flow and (b) Total heat accumulation

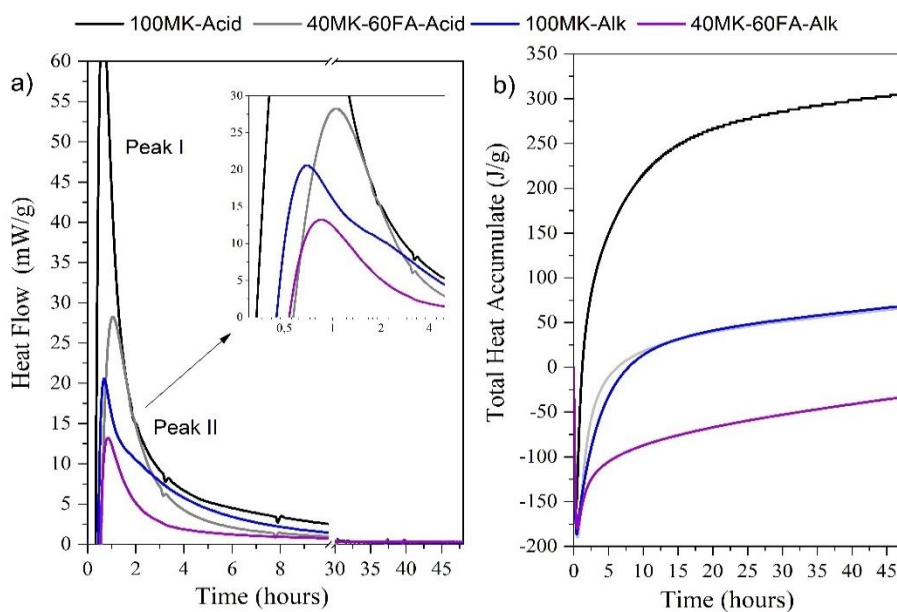
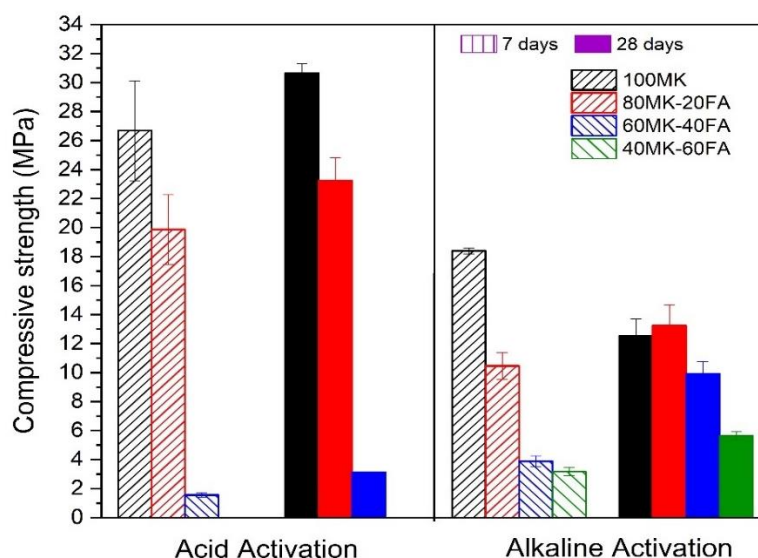


Figure 6 - Compressive strength at 7 and 28 days for all groups



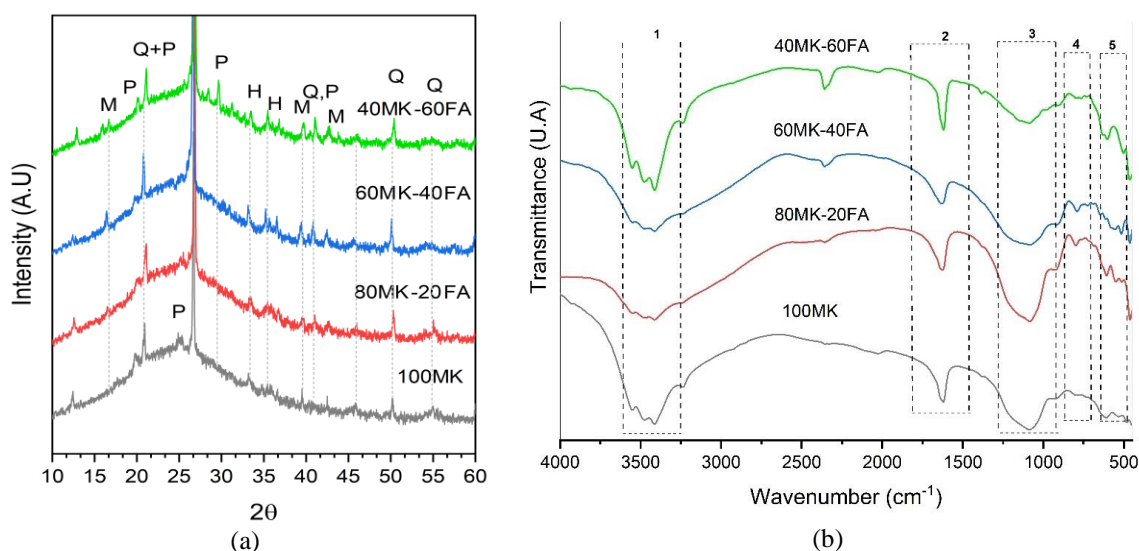


As the curing period progressed, alkaline activations exhibited a greater formation of rigid structures, resulting in a substantial increase in strength. Specifically, there was an approximately 155% and 80% increase in systems incorporating 40% and 60% FA, respectively. However, 100MK systems showed a drop at 28 days, this behavior is common on MK-paste due to shrinkage related to reaction products with low CaO (Huang; Wang, 2024). On the other hand, acid activations showed a more consistent increase in strength over time. For systems based on 100MK and 80MK, there was a constant increase of approximately 15% at 28 days. However, for the group with 60MK, although there was a significant increase in strength, it remained lower at 3.50 MPa. These observations underscore the distinct temporal evolution of compressive strength in acid and alkaline activation systems, with alkaline activations demonstrating a more pronounced improvement over time due to the formation of rigid structures.

Finally, XRD and FTIR spectrums were analyzed from samples at 28 days. The results are represented in Figure 7a and 7b for acid groups. About XRD characterization, Figure 7a, shows the amorphous halo linked to the formation of structures, that turn wider after activation, compared with the precursors in all groups, i.e., it is the indicator of phase phosphate aluminosilicate (Zulfikly *et al.*, 2021). Similarly to Guo *et al.* (2021), mixtures containing fly ash record this amorphous halo slightly wider than the 100MK group. However, it was also observed that certain crystalline phases as quartz and illite remain after activation, showing that they are unaffected by the treatment acid (Karuppaiyan; Jeyalakshmi, 2024). The Berlinite phase, or  $\text{AlPO}_4$ , appears together with quartz remaining (André *et al.*, 2023; Morsy *et al.*, 2019).

In addition, Figure 7b records the results obtained from FTIR analysis. Therein, several band regions named to #1 until #5 were identified. Band #1, located approximately between  $3226\text{--}3558\text{ cm}^{-1}$ , corresponds to the O-H group band. Band #2 located at  $1618\text{ cm}^{-1}$  is associated with angular deformation vibrations of the H-O-H band. As occurs in alkaline activations, this band indicates the presence of water molecules that are superficially absorbed or trapped in the large cavities of the polymeric network of the geopolymeric gel (Nobouassia *et al.*, 2022). Band #3, located at approximately  $1080\text{ cm}^{-1}$ , corresponds to the P-O asymmetric stretching and  $\text{PO}_2$  asymmetric stretching bond band of the P=O doubly bonded oxygen vibration of phosphoric acid (Zribi; Baklouti, 2021; Louati; Baklouti; Samet, 2016). According to Zribi and Baklouti (2021), the region between  $1300\text{ cm}^{-1}$  and  $900\text{ cm}^{-1}$  is very informative, as it can include different vibration modes of Si-O-P, Al-O-P. Band #4, located between  $980\text{ cm}^{-1}$  and  $780\text{ cm}^{-1}$ , represents the vibrations of the P-O-P bond, characteristic of the acidic geopolymeric system (Li *et al.*, 2022). Finally, band #5 corresponds to vibrations between  $600\text{ cm}^{-1}$  to  $550\text{ cm}^{-1}$  and corresponds to stretching vibrations of P-O-P and Al-O-P. The appearance of these new peaks indicates that the reaction of MK with  $\text{H}_3\text{PO}_4$  transforms the Si-O-Al structure in MK into Si-O-P, Si-O-Si and Al-O-P structures in the resulting acidic activation matrix (Lin *et al.*, 2021).

Figure 7 - (a) XRD and (b) FTIR results for acid activation group



Legend: P: Berlinite; Q: quartz; M: Mullite; and H: Hematite.

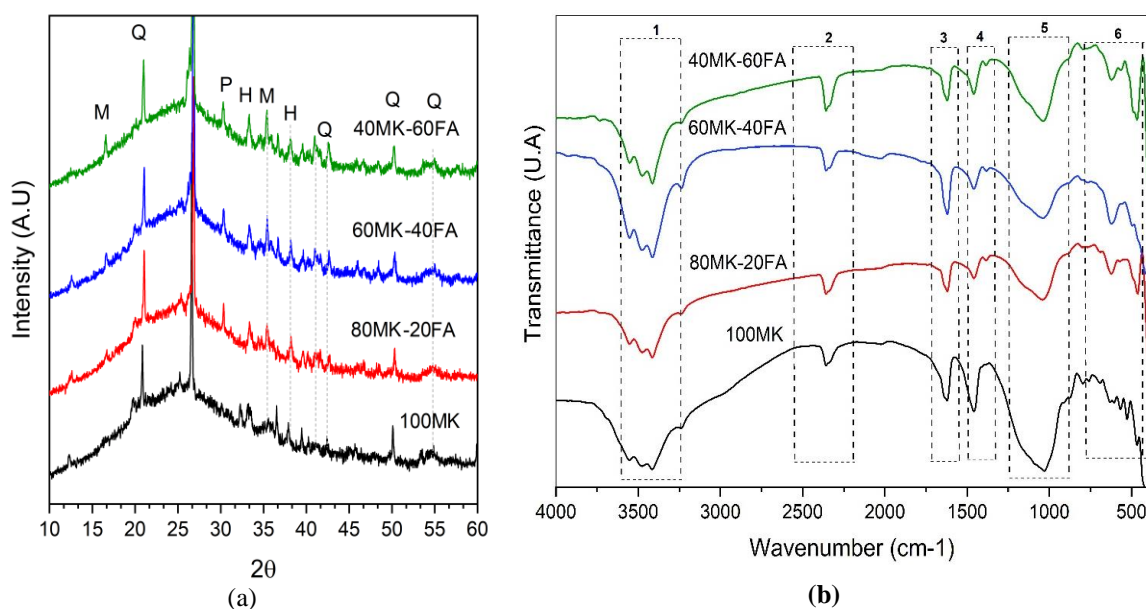
Regarding the XRD spectra of alkaline activations, see Figure 8a, the amorphous halo resulting from the formation of structures was recorded (Fernandez-Jimenes *et al.*, 2017). However, a significant contrast was also recorded. Initially, due to the intensity of the crystalline phases, which was greater than in acid activation, in the case of quartz, mullite and hematite. On the other hand, the illite peak disappeared under these conditions. This behavior indicates that even though the precursors are the same, the nature of the activation will lead to the reduction of certain phases, which depends mainly on the dissolution of the particles in the medium, which is a consequence of the concentration of the activator, the temperature, specific area and the energy of activation, as the barrier to be overcome to produce ionic exchange (Huang; Wang, 2024; Lin *et al.*, 2023).

Figure 8b shows the vibration peaks of the alkaline activation samples. As the same way, band # 1 and #2 correspond to O-H bond (Li *et al.*, 2023). As occurred in acid activation, the absorption band at 1611-1625  $\text{cm}^{-1}$  is associated with bending vibrations of carbon molecules. water H-O-H (Tchakouté; Ruscher, 2017). The band located in the area #4, at 1450  $\text{cm}^{-1}$ , corresponds to stretching of O-C-O, which implies formation of carbonate into geopolymers due to the reaction of free  $\text{Na}^+$  ions with atmospheric  $\text{CO}_2$  (Gao *et al.*, 2014). Band #5 of vibration at 1025  $\text{cm}^{-1}$  is associated with the Si-O-T bond (where T can refer to Al, Fe or Si). According to Tantonio *et al.* (2023), this band corresponds to the presence of the alkaline activation gel. The Si-O-Al and Si-O-Si bands and can be associated with the Silica tetrahedron ( $\text{SiO}_4$ ) (Tambara Junior; Cheriaf; Rocha, 2018).

## Conclusion

The acid activation of unitary and binary systems based on metakaolin and fly ash exhibits hardening and rheological behavior similar to alkaline activation systems. However, systems based on acid activation do not develop a second peak associated to polymerization at isothermal calorimetry. The presence of fly ash decreases substantially the kinetics reaction. Incorporating up to 20% fly ash is considered suitable for both systems. However, replacements greater than 40% fly ash are not recommended in an acid activation system because, under the evaluated conditions, they resulted in low or no compressive strength. In contrast, for alkaline activations, significant increases in compressive strength are observed over time, starting from the 20% incorporated content of fly ash in the system. This suggests that alkaline activations may be more resilient to higher levels of fly ash incorporation compared to acid activations.

Figure 8 - (a) XRD and (b) FTIR results for alkaline activation group



Legend: P: Phosphate; Q: quartzo; M: Mullite; and H: Hematite.



## References

- ABOULAYT, A. *et al.* Stability of a new geopolymer grout: rheological and mechanical performances of metakaolin-fly ash binary mixtures. **Construction and Building Materials**, v. 181, p. 420–436, 2018.
- ALVI, I. H. *et al.* A critical review of the advancements in acid-activated metakaolin geopolymers. **Construction and Building Materials**, v. 421, p. 0–3, 2024.
- ANDRÉ, R. A. *et al.* Analysis of the properties of chemically bound phosphate ceramics (CBPCs) produced from metakaolin with various acid phosphates. **Applied Clay Science**, v. 243, n. June, 2023.
- BU, M. *et al.* Dissolution behaviors and mechanisms of metakaolin in acidic activators. **Cement and Concrete Research**, v. 178, p. 107442, 2024.
- DEROUICHE, R.; BAKLOUTI, S. Phosphoric acid based geopolymerization: effect of the mechanochemical and the thermal activation of the kaolin. **Ceramics International**, v. 47, n. 10, p. 13446–13456, 2021.
- EISAZADEH, A.; KASSIM, K. A.; NUR, H. Stabilization of tropical kaolin soil with phosphoric acid and lime. **Natural Hazards**, v. 61, n. 3, p. 931–942, 2012.
- FERNÁNDEZ-JIMÉNEZ, A. *et al.* Sustainable alkali activated materials: precursor and activator derived from industrial wastes. **Journal of Cleaner Production**, v. 162, p. 1200–1209, 2017.
- GAO, K. *et al.* Effects SiO<sub>2</sub>/Na<sub>2</sub>O molar ratio on mechanical properties and the microstructure of nano-SiO<sub>2</sub> metakaolin-based geopolymers. **Construction and Building Materials**, v. 53, p. 503–510, 2014.
- GAO, L. *et al.* Effect of phosphoric acid content on the microstructure and compressive strength of phosphoric acid-based metakaolin geopolymers. **Heliyon**, v. 6, n. 4, p. e03853, 2020.
- GUNASEKARA, C.; SETUNGE, D. W. L., S.; SANJAYAN, J. G. Zeta potential, gel formation and compressive strength of low calcium fly ash geopolymers. **Construction and Building Materials**, v. 95, p. 592–599, 2015.
- GUO, H. *et al.* Preparation of high-performance silico-aluminophosphate geopolymers using fly ash and metakaolin as raw materials. **Applied Clay Science**, v. 204, n. October 2020, p. 106019, 2021.
- HE, M. *et al.* Strength, microstructure, CO<sub>2</sub> emission and economic analyses of low concentration phosphoric acid-activated fly ash geopolymer. **Construction and Building Materials**, v. 374, 2023.
- HUANG, Z.; WANG, Q. The effect of temperature on dissolution activity of fly ash and metakaolin in alkaline conditions. **Cement and Concrete Composites**, v. 146, p. 105363, 2024.
- KARUPPAIYAN, J.; JEYALAKSHMI, R. Dielectric response of alkali aluminosilicate hydrate and silico alumino phosphate network present in metakaolin – graphene oxide geopolymer: a comparative study. **Inorganic Chemistry Communications**, v. 161, p. 112036, 2024.
- KAZE, C. R. *et al.* Mechanical and physical properties of inorganic polymer cement made of iron-rich laterite and lateritic clay: a comparative study. **Cement and Concrete Research**, v. 140, n. May 2020, 2021.
- KRIEGSEIS, S. *et al.* Zeta potential and long-term stability correlation of carbon-based suspensions for material jetting. **Open Ceramics**, v. 4, p. 100037, 2020.
- LE-PING, L. *et al.* Preparation of phosphoric acid-based porous geopolymers. **Applied Clay Science**, v. 50, n. 4, p. 600–603, 2010.
- LI, J. *et al.* Properties and mechanism of high-magnesium nickel slag-fly ash based geopolymer activated by phosphoric acid. **Construction and Building Materials**, v. 345, n. May, p. 128256, 2022.
- LI, J. *et al.* The Effect of Bayer Red Mud Blending on the Mechanical Properties of Alkali-Activated Slag-Red Mud and the Mechanism. **Applied Sciences**, v. 13, p. 452, 2023.
- LIN, H. *et al.* Properties and reaction mechanism of phosphoric acid activated metakaolin geopolymer at varied curing temperatures. **Cement and Concrete Research**, v. 144, p. 106425, 2021.
- LIN, H. *et al.* Role of H<sub>3</sub>PO<sub>4</sub> concentration on the dissolution and reaction kinetics of phosphate acid based metakaolin geopolymer. **Journal of Non-Crystalline Solids**, v. 606, p. 122195, 2023.
- LOUATI, S.; BAKLOUTI, S.; SAMET, B. Acid based geopolymerization kinetics: effect of clay particle size. **Applied Clay Science**, v. 132–133, p. 571–578, 2016.

- LUZ, G. da *et al.* Effect of pristine and functionalized carbon nanotubes on microstructural, rheological, and mechanical behaviors of metakaolin-based geopolymer. **Cement and Concrete Composites**, v. 104, n. May, p. 103332, 2019.
- MEDINA, J.; GUIDA, H. N. Stabilization of lateritic soils with phosphoric acid. **Geotechnical and Geological Engineering**, v. 13, n. 4, p. 199–216, 1995.
- MICHAELS, A. S.; TAUSCH, F. W. **Phosphoric acid stabilization of fine-grained soils: improvements with secondary additives**. Washington, 1961. Available:  
<http://onlinepubs.trb.org/Onlinepubs/hrbulletin/282/282-003.pdf>. Access: 14 June 2023
- MORSY, M. S. *et al.* Potential use of limestone in metakaolin-based geopolymer activated with  $H_3PO_4$  for thermal insulation. **Construction and Building Materials**, v. 229, p. 117088, 2019.
- NOBOUASSIA, C. *et al.* Reaction kinetics and microstructural characteristics of iron-rich laterite-based phosphate binder. **Construction and Building Materials**, v. 320, p. 126302, 2022.
- PACHECO-TORGAL, F. *et al.* **Handbook of alkali-activated cements, mortars and concretes**. Cambridge: Elsevier, 2015.
- PEREIRA, K. R. O. **Ativação ácida e preparação de argilas organofílicas partindo-se de argila esmectítica proveniente do Estado da Paraíba**. Campina Grande, 2003. 95 f. Universidade Federal de Campina Grande, 2003. Dissertação de Mestrado.
- TABORDA-BARRAZA, M. *et al.* Evaluation of CNTs and SiC whiskers effect on the rheology and mechanical performance of metakaolin-based geopolymers. **Materials**, v. 15, n. 17, 2022.
- TAMBARA JÚNIOR, L. U. D.; CHERIAF, M.; ROCHA, J. C. Development of alkaline-activated self-leveling hybrid mortar ash-based composites. **Materials**, v. 11, n. 10, 2018.
- TANTONO, S. N. *et al.* Alkaline and acid activations of calcined laterites: a comparative study. **Silicon**, v. 15, s.n, p. 2797-2810, November 2022.
- TCHAKOUTÉ, H. K.; RÜSCHER, C. H. Mechanical and microstructural properties of metakaolin-based geopolymer cements from sodium waterglass and phosphoric acid solution as hardeners: a comparative study. **Applied Clay Science**, v. 140, p. 81–87, 2017.
- XIE, X. *et al.* Effect of acid-activator characteristics on the early hydration behavior and properties of metakaolin-based geopolymer. **Journal of Building Engineering**, v. 72, n. April, p. 106608, 2023.
- ZRIBI, M.; BAKLOUTI, S. Investigation of Phosphate based geopolymers formation mechanism. **Journal of Non-Crystalline Solids**, v. 562, p. 120777, 2021.
- ZRIBI, M.; SAMET, B.; AKLOUTI, S. Mechanical, microstructural and structural investigation of phosphate-based geopolymers with respect to P/Al molar ratio. **Journal of Solid State Chemistry**, v. 281, n. August 2019, p. 121025, 2020.
- ZULKIFLY, K. *et al.* Effect of phosphate addition on room-temperature-cured fly ash-metakaolin blend geopolymers. **Construction and Building Materials**, v. 270, p. 121486, 2021.

**Madeleing Taborda-Barraza**

Conceptualization, Methodology, Data curation, Data analysis, Writing original manuscript.

Departamento de Engenharia Civil | Universidade Federal de Santa Catarina | Rua João Piu Duarte Silva | Florianópolis - SC - Brasil | CEP 88037-001 | E-mail: madelatb@gmail.com

**Vanessa de Amorim Amorim**

Data curation, Data analysis, Writing-original draft.

Departamento de Engenharia Química e Alimentos | Universidade Federal de Santa Catarina | Rua do Biotério Central | Florianópolis - SC - Brasil | CEP 88037-010 | E-mail: vanessa.amorim2204@gmail.com

**Thais Marques da Silva**

Data curation, Data analysis, Writing-original draft.

Departamento de Engenharia Civil | Universidade Federal de Santa Catarina | E-mail: thaism21@ymail.com

**Philippe Jean Paul Gleize**

Methodology, Resources, Supervision, Data and Experiment Validation, Review.

Departamento de Engenharia Civil | Universidade Federal de Santa Catarina | E-mail: p.gleize@ufsc.br

Editor: **Enedir Ghisi**

Editora de seção: **Ana Paula Kirchheim**

***Ambiente Construído***

Revista da Associação Nacional de Tecnologia do Ambiente Construído

Av. Osvaldo Aranha, 99 - 3º andar, Centro

Porto Alegre - RS - Brasil

CEP 90035-190

Telefone: +55 (51) 3308-4084

[www.seer.ufrgs.br/ambienteconstruido](http://www.seer.ufrgs.br/ambienteconstruido)

[www.scielo.br/ac](http://www.scielo.br/ac)

E-mail: [ambienteconstruido@ufrgs.br](mailto:ambienteconstruido@ufrgs.br)



This is an open-access article distributed under the terms of the Creative Commons Attribution License.